文章编号：1001-9014(2020)02-0163-06

DOI:10. 11972/j. issn. 1001-9014. 2020. 02. 005

Design and experiments of 94 GHz Gyrotron for non-lethal biological effects of millimeter wave radiation

PAN Yuan-Yuan[1], WANG Li-Na[2*], LIU Jian-Wei[2], WANG Hui[2], CHEN Shuang[2]

(1. Department of Geriatric Cardiology, Sichuan Academy of Medical Sciences & Sichuan Provincial People's Hospital, Chengdu 610072, China;
2. School of Electronic Science and Engineering, University of Electronic Science and Technology of China, Chengdu 610054, China)

Abstract: The design and experiment of 94 GHz gyrotron with an inside quasi-optical system for the non-lethal biological effects of millimeter wave radiation are presented in this paper. The reason we chose $TE_{+6,2}$ mode as the experimental working mode is to reduce the wall heating problem at high power and high frequency. For a high-order mode, there are more neighboring modes, so mode competition affects the stability and effective operability of the experiment. The gradually tapered cavity has been designed to suppress mode competition in single cavities. In addition, the power conversion efficiency of the quasi-optical mode converter with low diffraction is 98. 54%. The experimental results confirm that the output power of 50. 9 kW is obtained with efficiency of 34. 3%. For the non-lethal biological effects, we can draw the conclusion that the overall scheme can achieved the expected results.

Key words: gyrotron, gradual taper cavity, quasi-optical mode converter, biological effects
PACS: 84. 40. Ik, 45. 55. Sa, 87. 50. Y-

用于毫米波辐射非致命生物效应的94 GHz回旋管设计与实验

潘媛媛[1], 王丽娜[2*], 刘建卫[2], 王 晖[2], 陈 爽[2]

(1. 四川省医学科学院&四川省人民医院老年心内科, 四川 成都 610072;
2. 电子科技大学 电子科学与工程学院, 四川 成都 610054)

摘要: 设计和测试了内嵌准光系统的94 GHz回旋管, 该系统主要用于研究毫米波辐射的非致命生物效应。为了减少大功率高频下的回旋管壁面加热问题, 选择$TE_{+6,2}$模式作为工作模式。对于高阶模式, 存在更多相邻模式, 因此模式竞争会影响实验的稳定性和有效的可操作性。渐变腔已被设计为抑制单个腔中的模式竞争。另外, 具有低衍射准光模式变换器的功率转换效率为98.54%。实验结果表明, 回旋管输出功率为50.9 kW, 效率为34.3%。对于非致死的生物效应研究, 整体设计方案达到了预期的效果。

关 键 词: 回旋管; 渐变腔体; 准光模式变换器; 生物效应

中图分类号: TN128 **文献标识码**: A

Introduction

Based on the working mechanism of electron cyclotron devices, high-power gyrotron tubes are the source of millimeter-wave and terahertz-wave radiation [1]. The advantage of the cyclotron relative to the Cherenkov device is that it provides a higher average power. In addition, the cyclotron can utilize an electron beam with lower energy of 10~100 keV [2]. Therefore, gyrotron is known as one of the most promising high-power sources [3-9] and its applications for spectrum, communication, high-resolution RADAR, biomedical and terahertz band technologies have great potential for development.

Due to the needs of the application, the gyrotron needs to work at higher frequencies, higher power and higher efficiency. At the same time, with the increase of

Received date: 2019- 12- 09, **revised date**: 2020- 01- 03 **收稿日期**: 2019- 12- 09, **修回日期**: 2020- 01- 03

Biography: PAN Yuan-Yuan, female, Chengdu, China, Head nurse. Research area involves cardiovascular nursing, nursing management and the biological effect produced by extremely high frequency. E-mail: pan__yuanyuan@126. com

* **Corresponding author**: E-mail: linaw2018@outlook. com

output power, the high-frequency structure of the gyrotron increases continuously, and it often works in the high-order mode, which brings difficulties to the transmission and mode conversion of electromagnetic waves. For example, for a gyrotron with an output power of 1 MW and a conversion efficiency of 50%, increasing the conversion efficiency by 1% means that the lost power will be reduced by 0.005 MW [10]. In view of the above reasons, we decided to use a quasi-optical mode converter to transmit electromagnetic waves at the output. The quasi-optical mode converter consists of a launcher and a mirror system. prebunching launchers are widely used in modern high power gyrotron tubes, such as periodic helical perturbation launchers [11-12], mirror-line launchers[13], and hybrid-type launchers [14]. Here, we adapt the periodic perturbation launcher because of an uptaper which can effectively reduce the reflected waves formed by the waveguide wall disturbance.

In recent years, the biological effects of millimeter wave radiation have attracted much attention. Because of its short wavelength and poor penetration, millimeter wave radiation is easily absorbed by tissues with more water content. Therefore, the local effects of millimeter wave radiation are mainly skin and eye damage effects. This study combines the rabbit behavior and skin damage effects in 94 GHz high power millimeter wave radiation, aiming to provide experimental basis for exploring the skin damage effects and mechanisms of high-power millimeter wave radiation.

The rest of this paper is organized as follows. In Sect. 1, this part starts with characteristics of mode selection. Then, one continues with the cold cavity design, followed by the hot cavity analysis. Subsequently, the magnetron injection gun is presented. The part concludes with the quasi-optical mode converter with high power efficiency and loss diffraction. The measured results of the gyrotron are shown in Sect. 2. Finally, one makes a summary in Sect. 4.

1 Theory and simulation

1.1 Mode selection and cold cavity analysis

In order to achieve greater output power, the operating mode should select a high-order mode of 94 GHz. The traditional low-order waveguide mode does not work well, but Higher-order modes cause mode competition. Therefore, it is necessary to study the relationship between working mode and cavity further. In order to suppress the parasitic mode near the working mode, a gradual cavity is used [15].

According to the result of numerical calculation, the diffraction quality factor of the main mode $TE_{6,2}$ is 1 150, and the resonance frequency is 94.19 GHz. The cross section of the optimized cavity with the radius Rc =5.96 mm, input port R_{in} =5.25 mm and output port R_{out} =7 mm are shown in Fig. 1 together with the normalized cold-cavity electric field distribution of the operating mode $TE_{6,2}$.

After the design of the cold cavity is completed, the appropriate beam radius should be carefully selected to

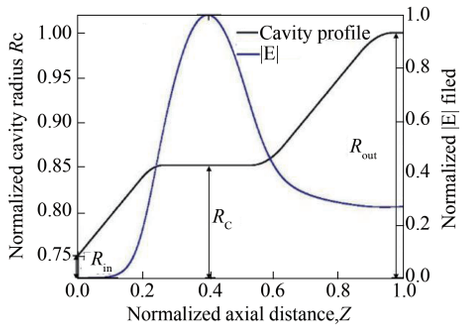

Fig. 1 The cavity structure and distribution of electric field relationship
图1 腔体结构与电场分布的关系图

achieve the purpose of suppressing the competition mode and obtaining a good beam-wave interaction between the main mode and the electron beam. According to the beam-wave coupling equation of Ref. 1, Fig. 2 shows the normalized coupling coefficient of the operating mode and the competitive mode as a function of beam radius. One can obtain the $TE_{+6,2}$ mode (co-rotating mode) produces strong coupling with the electron beam at a radius of 3.3 mm, and the $TE_{-6,2}$ mode (counter-rotating mode) produces a strong coupling at a radius of 4.3 mm. By comparing the radius of the two modes, the beam radius of the 4.3 mm beam in the $TE_{-6,2}$ mode is close to the cavity radius of 5.96 mm, so that electrons will more easily enter the inner wall of the cavity. Based on the above analysis, we chose a co-rotation mode with a beam radius of 3.3 mm.

By analyzing Fig. 2, when the beam radius is 3.3 mm, the modes $TE_{-4,3}$, $TE_{0,3}$, $TE_{-3,3}$, $TE_{-2,3}$ and $TE_{2,3}$ become the main competition modes. Therefore, we further study the starting current of the competition modes to solve the mode competition. According to the starting current theory of Ref. 14, Fig. 3 shows the starting current of the operating mode and the competitive mode as a function of the external magnetic field, where the beam voltage of 40 kV, beam radius of 3.3 mm and transverse-to-axial velocity ratio of 1.3 were selected in the calculation.

As shown, the $TE_{+6,2}$ mode can be started separately in the appropriate magnetic field range. By changing the external magnetic field, the purpose of suppressing the competition mode can be achieved. In summary, we can think of the $TE_{+6,2}$ mode as the desired gyrotron normal mode of operation.

1.2 Analysis of multi-mode beam-wave interaction

After the design of cold-cavity and the studies of linear analysis, one need to the beam-wave interaction. Multi-mode simulation of a 94 GHz single-cavity gyrotron using the in-house developed non-linear time-dependent code [16]. We ignore the propagation velocity and space charge effect of electron beams[17]. It is assumed that all electrons in the loop bundle have the same center radius. In the selection of competing modes in the simulation, the modes that the resonator frequency is between 90

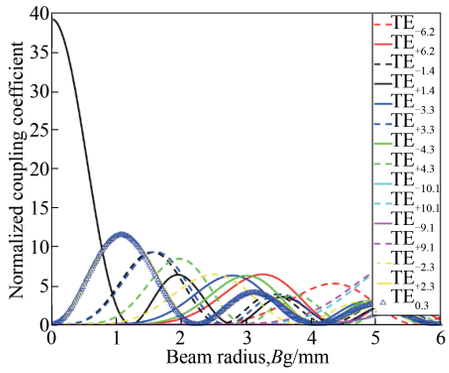

Fig. 2 The normalized beam-wave coupling coefficient of the dominant and competitive modes varies with beam radius
图2 主模和竞争模式的归一化注波耦合系数随波束半径变化

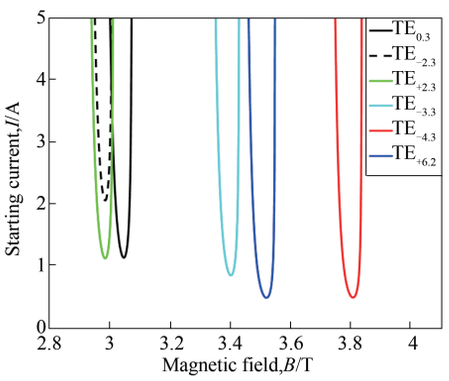

Fig. 3 The starting current of the operating mode and the main competitive mode varies with the external magnetic field, where the beam voltage of 30 kV, beam radius of 3. 3 mm and transverse-to-axial velocity ratio of 1. 3 were selected
图3 工作模式和主要竞争模式的起振电流随外磁场变化,其中选取了30 kV的电子注电压、3. 3 mm的电子注半径和1. 3的横轴速比

GHz and 100 GHz and the beam-wave coupling of relative to the main mode is greater than 70% were selected. The startup simulation is shown in the Fig. 4. As it shows that the main mode $TE_{+6,2}$ can reach at stable steady with the output power of 62 kW under the conditions of beam voltage of 40 kV, beam current of 4 A, transverse-to-axial velocity ratio of 1. 3, beam radius of 3. 3 mm.

1. 3 Study of Magnetron Injection Gun

According to the requirements of output power and efficiency, the best parameters of electron beam are given by the simulation results of the interaction cavity. The optimum value of the electron beam parameters is also given. Based on the theory of electron guns, the goal of MIG design is to emit electron beams at specific radial positions. Meanwhile, the electron beam has minimum velocity spread and the best velocity ratio. In view of these objectives, the optimized parameters include: cathode and anode geometry, the gap between them, the tilt length of the cathode, the cathode tilt angle, the cathode magnetic field distribution, and the anode voltage. In order to meet the parameters of the gyrotron, we developed a numerical code for designing the MIG and calculated the lateral velocity and longitudinal velocity distribution

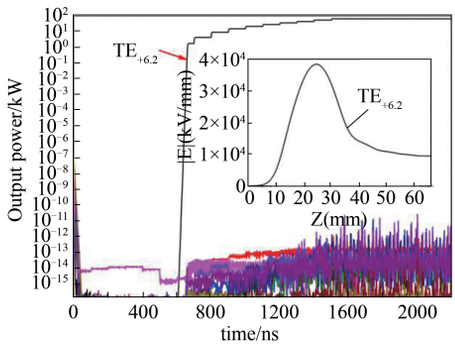

Fig. 4 The startup of multi-mode beam-wave interaction, where the beam voltage of 40 kV, beam current of 4A, transverse-to-axial velocity ratio of 1. 3, beam radius of 3. 3 mm
图4 多模式注波相互作用的起振,其中电子注电压为40 kV,电子注电流为4 A,横轴速度比为1. 3,电子注半径为3. 3 mm

to be 2. 7% and 4. 0%. The trajectories and structure are shown in Fig. 5. The specific parameters of optimized beam are presented in Table 1.

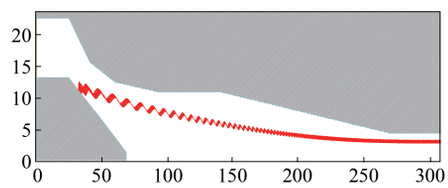

Fig. 5 The trajectory and structure of the designed MIG
图5 设计的磁控注入枪的轨迹和结构

Table 1 Optimized beam parameters and MIG geometry
表1 优化的电子注参数和磁控注入枪的几何结构

Parameters	Values
Beam voltage	40 kV
beam current	4 A
average radius	3. 3 mm
Beam pitch ratio	1. 3
Cavity Magnetic field	3. 540 T

1. 4 Quasi-optical mode converter

One has developed a high power gyrotron operating at a frequency of 94 GHz $TE_{6,2}$ mode. Due to the high output power, when the electromagnetic field is output longitudinally, a heat distribution pattern is formed on the output window in the form of $TE_{6,2}$, which is unevenly distributed and is prone to stress and causes the output window to rupture. At the same time, the $TE_{6,2}$ mode electromagnetic waves directly output from the circular waveguide are distributed in a conical distribution in free space and cannot be directly utilized. Therefore, this paper uses a Denisov type launcher and four prebunching mirrors to improve the utility of the gyrotron and convert $TE_{6,2}$ into a fundamental Gaussian mode.

A harmonically deformed launcher is used in the system [18]. Disturbance of the waveguide wall changes the boundary conditions of the inner wall of the waveguide. The eigen modes in a circular waveguide will cou-

ple with other modes. The mutual coupling and superposition of modes will form a new field distribution. Table 2 shows the relative power of the 9 modes that form the Gaussian distribution [19].

Table 2 The relative power distribution of the 9 modes that form the Gaussian distribution
表2 构成高斯分布9个模式的相对功率分布

$TE_{4,3}$	$TE_{7,2}$	$TE_{10,1}$
3%	11%	3%
$TE_{3,3}$	$TE_{6,2}$	$TE_{9,1}$
11%	44%	11%
$TE_{2,3}$	$TE_{5,2}$	$TE_{8,1}$
3%	11%	3%

Optimizing the perturbation of the waveguide wall enables a specific Gaussian field distribution to be obtained. Therefore, the design of the specific structural parameters of the launcher is very important. The radius of the launcher is different at each position (ϕ, z). The change in radius can be expressed by the following formula

$$\Delta R = \delta_1 \cos\left(\Delta\beta_1 z - l_1\varphi\right) + \delta_2\cos\left(\Delta\beta_2 z - l_2\varphi\right), \quad (1)$$

where φ is the azimuthal angle, δ_1 is the longitudinal disturbance amplitude, and δ_2 is the azimuth disturbance amplitude. $\Delta\beta_1$ is half of the longitudinal wavenumber difference between the longitudinal coupling modes, z is the longitudinal position and $\Delta\beta_2$ is half of the longitudinal wavenumber difference between the azimuthal coupling modes. l_1 and l_2 are the azimuth disturbance periods of the longitudinal disturbance term and the azimuth disturbance term, respectively.

$$R = R_0 + \alpha z + \Delta R \quad , \quad (2)$$

where R_0 is the initial radius of the circular waveguide, R_0 =7.07 mm, t is the slope of wall radius taper of the launcher, α = 0.003.

The wave beam is radiated from the launcher and propagates through a reflection system consisting of a four-sided mirror to the output window. The first mirror is an elliptical mirror, the second mirror is a parabolic mirror, and the other two mirrors are phase correcting mirrors. Both correction mirrors satisfy the Katsenelenbaum-Semenov algorithm. The mirror system adjusts the shape, convergence, and direction of the Gaussian beam to achieve enough energy for non-fatal biological effects.

After the analysis of the basic theory, we create a model in the FEKO (Electromagnetic simulation software). It is shown in Fig. 6. The electromagnetic wave is transmitted by following our prescribed route and one can obtain good Gaussian mode in the position of output window in Fig. 7.

According to the above theoretical analysis and numerical simulation, the Gaussian content of the outgoing wave beam to the target function at the output window is about 93%, and the conversion efficiency of the entire mode converter is about 98.54%.

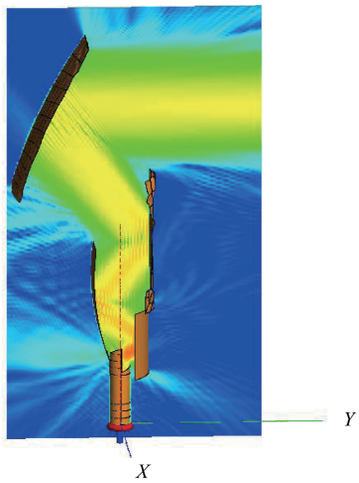

Fig. 6 Overall diagram of electromagnetic wave transmission process on YOZ plane
图6 YOZ平面电磁波传播过程总体示意图

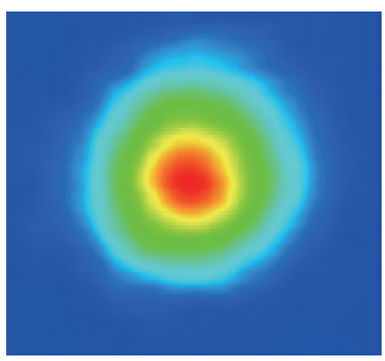

Fig. 7 output window field distribution by Electromagnetic simulation
图7 电磁仿真输出窗口处场分布

2 Experimental results

2.1 The results of gyrotron

The corresponding W-band gyrotron is designed and manufactured using the above simulation results. The gyrotron has a single-anode magnetron injection gun, single cavity and single stage recessed collector.

Table 3 Data from the experimental test
表3 实验测试数据

Parameters	Values
Cathode voltage	41.2 kV
Cathode current	3.6 A
Anode voltage	8 kV
Frequency	94.03 GHz
Output power	50.9 kW

In Table 3, we list the parameter data for the experimental test. Combining the analytical results with the test results, we know that there is a 4.45% error between the two. The reason for the error formation is mainly that the calculation results are obtained under ideal condi-

tions. For example, in the simulation calculation, the velocity spread, the deviation of the guiding center radius, and the space charge effect are ignored. In summary, since the simulation calculation is only 4.45% deviation from the actual experiment, we believe that the simulation reasonably describes the experimental results. The calculation results based on the nonlinear coupled equation can be used to study the nonlinear interaction in the gyrotron.

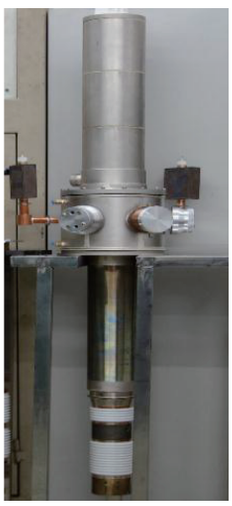

Fig. 8 Photo of the designed gyrotron with quasi-optical mode converter
图8 设计的内嵌准光学模式转换器回旋管图片

The gyrotron with quasi-optical mode converter is shown in Fig. 8. The white paper was placed at 0.6 m from the output window for 3 seconds. The output beam of the gyrotron is radiated to white paper, and it began to burn, forming a coin-sized spot which the field mode is shown in Fig. 9. Obviously, observing the burnt white paper, the center of the spot appears white, which is consistent with the amplitude profile of the Gaussian beam.

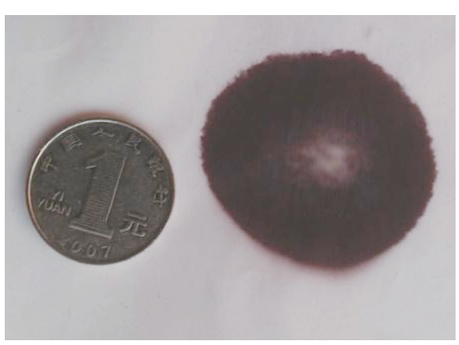

Fig. 9 The field pattern on a piece of paper at 0.6m from the gyrotron output window
图9 距回旋管输出窗口0.6 m的热敏纸上的场模式分布

2.2 Results of microwave action on non-fatal biological effects

As we can see in Fig. 10, the rabbit's neck was fixed on a wooden board and placed at a vertical position with a power density of 6.0 W/cm^2 below the gyrotron output port. We use the 94 GHz high-power millimeter wave source developed above, and the radiation duration is 30 s. After 20 seconds of radiation, the rabbit facial expression was painful and intermittent screams. As the radiation time prolonged, there were continuous behaviors such as body tremors, sharp head rotations, and limb struggles.

Fig. 10 Rabbit fixed on a wooden board
图10 固定在木板上的兔子

3 Summary

This paper designs a 94 GHz gyrotron for non-fatal biological effects. The experiment achieved a 50.9 kW operation with a Gaussian beam output. Based on the steady nonlinear self- consistent field theory, 34.3% of the interaction efficiency can be obtained by using TE6, 2 as the working mode. To get good output power, we use a system consisting of a transmitter and four mirrors to focus the beam while adjusting the wave front phase to avoid divergence and side lobes in the output beam. The energy of the launcher is transmitted to the output window through the mirror system, achieving a power transmission efficiency of 98.54% or more.

The experimental results show that a high efficiency gyrotron can be obtained in practical applications if certain conditions are met. For this non-fatal biological effect test, we can draw conclusions that the overall scheme can 6 W/cm2 of 94 GHz high-power millimeter-wave radiation causes rabbit skin recoverable damage. The degree of damage increases with increasing radiation dose, which provides an experimental basis for further research.

Acknowledgment

The corresponding author is Lina Wang and her E-mail is linaw2018@outlook.com. This work was supported in part by the Fundamental Research Funds for the Central Universities under Grant No. ZYGX2018J032, in part by the National Natural Science Foundation of China (Grant No. 61801088) and in part by the National Key R&D Program of China, contract numbers

2017YFE0300200 and 2017YFE0300201.

References

[1] Kartikeyan M V, Bore E, Thumm M K A. *Gyrotrons high power microwave and millimeter wave technology*[M]. Springer-Verlag, New York, NY, USA, 2004.

[2] Glyavin M Y, Ginzburg N S, Goldenberg A L, *et al*. THz gyrotrons: status and possible optimizations[J]. *Terahertz Sci. Tech*. 2012, **5**(2):67-77.

[3] Weide D. Applications and outlook for electronic terahertz technology[J]. *Opt.Photonics News*, 2003, **14**(4):48-53.

[4] Siegel P H. Terahertz technology in biology and medicine[J]. *IEEE Trans. Microw Theory Tech*. 2004, **52**(10):2438-2447.

[5] Granatstein V L, Nusinovich G S. Detecting excess ionizing radiation by electromagnetic breakdown of air[J]. J. *Appl. Phys*. 2010, **108**(6):063304-063309.

[6] Sabchevski S, Idehara T. Development of sub-terahertz gyrotrons for novel application[C]. In: Proceedings of the 36th International Conference Infrared, Millim. *Terahertz Waves*, 2011, pp. 1-2.

[7] Woolard D L, Brown E R, Pepper M, *et al*. Terahertz frequency sensing and imaging: A time of reckoning future applications[J]. *Proceedings of the IEEE*, 2005, **93**(10):1722-1743.

[8] Zhao Q X, Sheng Y. The nonlinear designs and experiments on a 0.42-THz second harmonic gyrotron with complex cavity[J]. *IEEE Transactions on Electron Devices*, 2017, **64**(2):564-570.

[9] Guo G, Niu X, Liu Y, *et al*. Modeling, simulation, and fabrication of electron optic system for application on 105 GHz high-power gyrotron[J]. *International Journal of Numerical Modelling: Electronic Networks, Devices and Fields*, 2019, p. e2593.

[10] Zhao G, Xue Q Z, Wang Y, *et al*. Design of quasi-optical mode converter for 170-GHz TE32, 9-Mode high-power gyrotron[J]. *IEEE Transactions on Plasma Science*, 2019, **47**(5):2582-2589.

[11] Denisov G G, Petelin M I, Vinogradov D V, *et al*. Converter of high-mode of a circular waveguide into the main mode of a mirror line[J]. W090/0780 HOIPI/l6, *PCT Gazette*, 1990, **16**:47-49.

[12] Dmitry V, Denisov G G, Petelin M I. Effective conversion of high waveguide modes to eigenwaves of open mirror lines[J]. *In Proc. 17th Int. Conf. Infr. Millim. Waves, Dec*. 1992, Art. *no*. 19291S.

[13] Jin J, Thumm M, Piosczyk B, *et al*. Novel numerical method for the analysis and synthesis of the fields in highly oversized waveguide mode converters[J]. *IEEE Trans. Microw. Theory Tech.*, 2009, **57**(7):1661-1668.

[14] Jin J, Thumm M, Gantenbein G, *et al*. A numerical synthesis method for hybrid-type high-power gyrotron launchers[J]. *IEEE Trans. Microw. Theory Techn*. 2017, **65**(3):699-706.

[15] Niu X, Lei C, Liu Y, *et al*. A study on 94 GHz low-voltage, low-current gyrotron[J]. *IEEE Transactions on Electron Devices*, 2013, **60**(11):3907-3912.

[16] Liu Q, Liu Y, Niu X, *et al*. Theoretical investigation on a multifrequency multimode gyrotron at Ka-band[J]. *IEEE Transactions on Plasma Science*, 2017, **45**(11):2955-2961.

[17] Ruifeng P, Nusinovich G S, Sinitsyn O V, *et al*. Numerical study of efficiency for a 670GHz gyrotron[J]. *Phys. Plasmas*. 2011, **18**:023107.

[18] Bogdashov A, Denisov G G. Asymptotic theory of high-efficiency converters of higher-order waveguide modes into eigenwaves of open mirror lines[J]. *Radiophys. Quant. Electon.*, 2004, **47**(4):283-296.

[19] Jin J B, Piosczyk B, Thumm M, *et al*. Quasi-optical mode converter/mirror system for a high-power coaxial-cavity gyrotron[J]. *IEEE Trans. Plasma Sci.*, 2006, **34**(4):1508-1515.